

# Orbital Degeneracy and Peierls Instability in Triangular Lattice Superconductor $\text{Ir}_{1-x}\text{Pt}_x\text{Te}_2$

Daiki Ootsuki<sup>1</sup>, Yuki Wakisaka<sup>2</sup>, Sunseng Pyon<sup>3</sup>, Kazutaka Kudo<sup>3</sup>, Minoru Nohara<sup>3</sup>, Masashi Arita<sup>4</sup>, Hiroaki Anzai<sup>4</sup>, Hirofumi Namatame<sup>4</sup>, Masaki Taniguchi<sup>4,5</sup>, Naurang L. Saini<sup>6,2</sup>, and Takashi Mizokawa<sup>2,1</sup>

<sup>1</sup>*Department of Physics, University of Tokyo, 5-1-5 Kashiwanoha, Chiba 277-8561, Japan*

<sup>2</sup>*Department of Complexity Science and Engineering,  
University of Tokyo, 5-1-5 Kashiwanoha, Chiba 277-8561, Japan*

<sup>3</sup>*Department of Physics, Okayama University, Kita-ku, Okayama 700-8530, Japan*

<sup>4</sup>*Hiroshima Synchrotron Radiation Center, Hiroshima University, Higashi-hiroshima 739-0046, Japan*

<sup>5</sup>*Graduate School of Science, Hiroshima University, Higashi-hiroshima 739-8526, Japan and*

<sup>6</sup>*Department of Physics, University of Roma "La Sapienza" Piazzale Aldo Moro 2, 00185 Roma, Italy*

(Dated: February 26, 2013)

We have studied electronic structure of triangular lattice  $\text{Ir}_{1-x}\text{Pt}_x\text{Te}_2$  superconductor using photoemission spectroscopy and model calculations. Ir 4*f* core-level photoemission spectra show that Ir 5*d*  $t_{2g}$  charge modulation established in the low temperature phase of  $\text{IrTe}_2$  is suppressed by Pt doping. This observation indicates that the suppression of charge modulation is related to the emergence of superconductivity. Valence-band photoemission spectra of  $\text{IrTe}_2$  suggest that the Ir 5*d* charge modulation is accompanied by Ir 5*d* orbital reconstruction. Based on the photoemission results and model calculations, we argue that the orbitally-induced Peierls effect governs the charge and orbital instability in the  $\text{Ir}_{1-x}\text{Pt}_x\text{Te}_2$ .

PACS numbers: 74.70.Xa, 74.25.Jb, 71.30.+h, 71.20.-b

## I. INTRODUCTION

Fe pnictides and chalcogenides, including  $\text{LaFeAsO}_{1-x}\text{F}_x$ <sup>1,2</sup> and  $\text{FeSe}_{1-x}\text{Te}_x$ ,<sup>3,4</sup> show an interesting interplay between superconductivity and magnetism which is deeply related to the multi-band structure derived from the Fe 3*d* orbitals. Recently, Pyon *et al.* have reported superconductivity in triangular lattice  $\text{IrTe}_2$  [see Fig. 1(a)] when Pt is substituted for Ir.<sup>5</sup> Interestingly, the parent material  $\text{IrTe}_2$  shows a structural phase transition at  $\sim 250$  K which is probably due to Ir 5*d*  $t_{2g}$  orbital order or bond order.<sup>6</sup> The Pt doping suppresses the static orbital or bond order, and the superconductivity appears around the quantum critical point where the orbital or bond order disappears. The comparison of superconductivity in triangular lattice  $\text{IrTe}_2$  and square lattice Fe pnictides/chalcogenides is very interesting and may provide clues to understand the mechanism of superconductivities in these materials. In addition, orbital effect on Fe pnictides/chalcogenides superconductors is currently under hot debate. Particularly, the Fe 3*d*  $yz/zz$  orbital degeneracy in the tetragonal phase of Fe pnictides/chalcogenides is similar to the Ir 5*d*  $yz/zz$  orbital degeneracy of the trigonal phase of  $\text{Ir}_{1-x}\text{Pt}_x\text{Te}_2$  although the Ir 5*d* spin-orbit interaction provides some differences. Therefore, study of orbital effect on  $\text{Ir}_{1-x}\text{Pt}_x\text{Te}_2$  is highly interesting and important.

$\text{IrTe}_2$  and  $\text{PtTe}_2$ , which have  $d^5$  configuration of  $\text{Ir}^{4+}$  ions and  $d^6$  configuration of  $\text{Pt}^{4+}$  ions respectively, crystallize into the  $\text{CdI}_2$ -type structure as shown in Fig. 1(a).  $\text{IrTe}_2$  exhibits a structural phase transition at  $\sim 250$  K from the trigonal ( $P3m-1$ ) to a monoclinic ( $C2/m$ ) structure, accompanied by temperature dependent anomaly

of electrical resistivity and magnetic susceptibility. On the other hand,  $\text{PtTe}_2$  with the trigonal structure does not exhibit the structural phase transition.<sup>6</sup> While no superconductivity has been reported for  $\text{IrTe}_2$  and  $\text{PtTe}_2$ ,<sup>8,9</sup> trigonal  $\text{Ir}_{1-x}\text{Pt}_x\text{Te}_2$  shows the superconductivity in the vicinity of the monoclinic phase.<sup>5</sup> The structural phase transition of  $\text{IrTe}_2$  would be related to the orbital degeneracy of the  $\text{Ir}^{4+}(d^5)$  state as shown in Fig. 1(b) and has similarity to the structural transition of spinel-type  $\text{CuIr}_2\text{S}_4$ .<sup>10-12</sup> In this paper, we report core-level and valence-band photoemission spectroscopy of triangular lattice  $\text{Ir}_{1-x}\text{Pt}_x\text{Te}_2$  superconductor. Photoemission results and model calculations indicate that the orbitally-induced Peierls effect plays an important role in the charge-orbital instability and the superconductivity of  $\text{Ir}_{1-x}\text{Pt}_x\text{Te}_2$ .

## II. METHODS

### A. Experiment

The polycrystalline samples of  $\text{Ir}_{1-x}\text{Pt}_x\text{Te}_2$  ( $x = 0.00, 0.03$ , and  $0.04$ ) were prepared as reported in ref. 5.<sup>5</sup>  $\text{IrTe}_2$  is nonsuperconducting while  $\text{Ir}_{1-x}\text{Pt}_x\text{Te}_2$  ( $x = 0.03$ , and  $0.04$ ) are superconducting with  $T_c = 3.1$  K and  $2.9$  K respectively. The photoemission measurements were performed at beamline 9A, Hiroshima Synchrotron Radiation Center using a SCIENTA R4000 analyzer with circularly polarized light. The total energy resolution was set to 8 meV for the selected excitation energy of  $h\nu = 10$  eV. The angular resolution was set to  $\sim 0.3^\circ$  that gives the momentum resolution of  $\sim 0.01 \text{ \AA}^{-1}$  for  $h\nu = 10$  eV. The circular polarization of the incident beam is  $50^\circ$  off

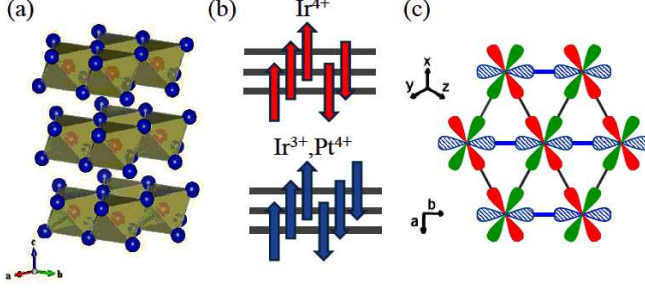


FIG. 1: (color online) (a) Crystal structure of IrTe<sub>2</sub> that was visualized by using the software package VESTA.<sup>7</sup> The IrTe<sub>6</sub> octahedra share their edges and form the IrTe<sub>2</sub> triangular lattice layer. (b) Electronic configurations of Ir<sup>4+</sup> (*d*<sup>5</sup>) and Ir<sup>3+</sup>, Pt<sup>4+</sup> (*d*<sup>6</sup>). (c) Ir 5*d* *t*<sub>2*g*</sub> orbitals on the triangular lattice. The thicker lines indicate shorter Ir-Ir bonds which are due to bond formation of the shaded Ir 5*d* *yz* orbitals.

the sample surface. The base pressure of the spectrometer was in the 10<sup>-9</sup> Pa range. The polycrystalline samples of Ir<sub>1-x</sub>Pt<sub>x</sub>Te<sub>2</sub> were fractured at 300 K under the ultrahigh vacuum and the spectra were acquired within 6 hours after the fracturing. The x-ray photoemission spectroscopy (XPS) was carried out at 300 K and 40 K using JEOL JPS9200 analyzer. Monochromatic Al K $\alpha$  (1486.6 eV) was used as x-ray source. The total energy resolution was about 0.6 eV. The base pressure of the chamber was in the 10<sup>-7</sup> Pa range. The binding energy was calibrated using the Au 4*f* core level of the gold reference sample. We fractured the polycrystalline samples of Ir<sub>1-x</sub>Pt<sub>x</sub>Te<sub>2</sub> at 300 K for the XPS measurements.

### B. Calculation

The electronic structure of IrTe<sub>2</sub> was analyzed using a tight-binding model with Ir 5*d* and Te 5*p* orbitals. The tight-binding Hamiltonian of the multi-band model<sup>13</sup> is given by

$$\begin{aligned}
 H &= H_p + H_d + H_{pd}, \\
 H_p &= \sum_{k,l,\sigma} \epsilon^p p_{k,l\sigma}^+ p_{k,l\sigma} + \sum_{k,l>l',\sigma} V_{k,ll'}^{pp} p_{k,l\sigma}^+ p_{k,l'\sigma} + H.c., \\
 H_d &= \sum_{i,m\sigma} \epsilon_d d_{i,m\sigma}^+ d_{i,m\sigma} + \sum_{i,m,m',\sigma,\sigma'} h_{mm'\sigma\sigma'}^d d_{i,m\sigma}^+ d_{i,m'\sigma'} \\
 &\quad + \sum_{k,m>m',\sigma} V_{k,mm'}^{dd} d_{k,m\sigma}^+ d_{k,m'\sigma} + H.c., \\
 H_{pd} &= \sum_{k,m,l,\sigma} V_{k,lm}^{pd} d_{k,m\sigma}^+ p_{k,l\sigma} + H.c.
 \end{aligned}$$

Here,  $d_{i,m\sigma}^+$  are creation operators for the Ir 5*d* electrons with orbital *m* and spin  $\sigma$  at site *i*.  $d_{k,m\sigma}^+$  and  $p_{k,l\sigma}^+$  are creation operators for Bloch electrons with momentum *k* which are constructed from the *m*-th component of the Ir 5*d* orbitals and from the *l*-th component of the Te 5*p* orbitals, respectively.  $h_{mm'\sigma\sigma'}^d$  represents the ligand field splitting and the atomic spin-orbit interaction for the Ir 5*d* orbitals. The transfer integrals  $V_{k,lm}^{pd}$  between the Ir 5*d* and Te 5*p* orbitals are given by Slater-Koster parameters (pd $\sigma$ ) and (pd $\pi$ ) which are set to -2.0 eV and 0.9 eV for the undistorted trigonal structure. Also the Te 5*p*-Te 5*p* transfer integrals  $V_{k,ll'}^{pp}$  are given by (pp $\sigma$ ) and (pp $\pi$ ) of 0.6 eV and -0.15 eV, and the Ir 5*d*-Ir 5*d* transfer integrals  $V_{k,mm'}^{dd}$  are given by (dd $\sigma$ ) and (dd $\pi$ ) of -0.4 eV and 0.15 eV for the undistorted trigonal structure. The magnitude of the Ir 5*d* spin-orbit interaction is set to 0.6 eV. When the trigonal structure is distorted, the Slater-Koster parameters are modified using the Harrison's rule.<sup>13</sup> The effect of orbital or bond order can be examined by introducing the 5% bond compression along the *b*-axis which is consistent with the experimental value. The transfer integrals along the *b*-axis are enhanced by the bond compression and, consequently, the degeneracy of the Ir 5*d* *t*<sub>2*g*</sub> bands can be removed. This can be viewed as a kind of band Jahn-Teller effect. The band Jahn-Teller effect modifies the Fermi surface geometry to cause Peierls instability in the orbitally-induced Peierls mechanism. The Te 5*p*-to-Ir 5*d* charge-transfer energy  $\Delta$  ( $= \epsilon^d - \epsilon^p$ ) is taken as an adjustable parameter to reproduce the spectral weight suppression at -0.1 eV by the lattice distortion.

### III. RESULTS AND DISCUSSION

Ir 4*f* and Te 3*d* core-level photoemission spectra of Ir<sub>1-x</sub>Pt<sub>x</sub>Te<sub>2</sub> (*x* = 0.00, 0.03, and 0.04) are displayed in Fig. 2. For *x* = 0.03 and 0.04, the Te 3*d* peaks are accompanied by shoulders at  $\sim$  575 eV which can be attributed to Te impurities at grain boundaries. The absence of this shoulder for IrTe<sub>2</sub> indicates that the photoemission results for IrTe<sub>2</sub> are highly reliable. As for the Pt doped samples, since the main Te 3*d* peaks representing the bulk Ir<sub>1-x</sub>Pt<sub>x</sub>Te<sub>2</sub> are still dominant, the Ir 4*f* and valence-band photoemission results can be used to discuss the bulk electronic structure. As shown in Fig. 2(a), the Ir 4*f* peak width of IrTe<sub>2</sub> slightly increases in going from 300 K to 40 K while those of the Pt doped samples as well as the Te 3*d* peaks do not show any such changes with temperature. The increase of peak width indicates that the density of Ir 5*d* *t*<sub>2*g*</sub> electrons is modulated in the low temperature phase of IrTe<sub>2</sub>. Here, it should be noted that the Ir 4*f* peak width increase of IrTe<sub>2</sub> is comparable to that of CuIr<sub>2</sub>S<sub>4</sub> in which the octamer Ir<sup>3+</sup>/Ir<sup>4+</sup> charge ordering was established<sup>11</sup> and the charge difference between the Ir<sup>3+</sup> site and the Ir<sup>4+</sup> site was observed in the Ir 4*f* XPS.<sup>12</sup>

On the other hand, the Ir 4*f* peak width of the Pt

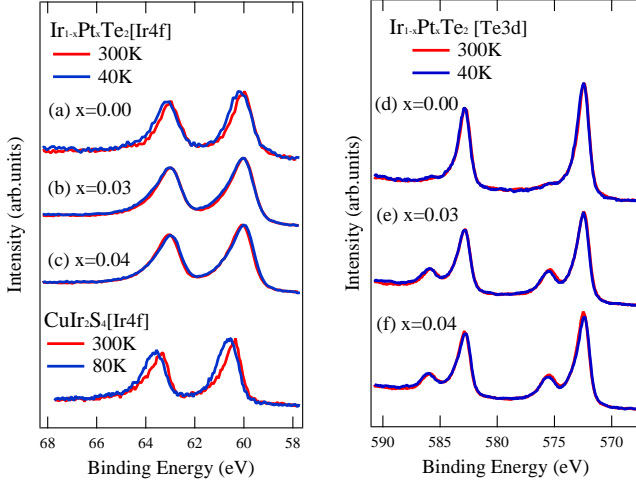


FIG. 2: (color online) Ir  $4f$  core-level photoemission spectra of  $\text{Ir}_{1-x}\text{Pt}_x\text{Te}_2$  for (a)  $x = 0.00$ , (b)  $x = 0.03$ , and (c)  $x = 0.04$  compared to that of  $\text{CuIr}_2\text{S}_4$ .<sup>12</sup> Te  $3d$  core-level photoemission spectra for (d)  $x = 0.00$ , (e)  $x = 0.03$ , and (f)  $x = 0.04$ .

doped samples does not change appreciably with temperature, indicating that the Ir  $5d$  charge modulation is suppressed by the Pt doping. Also the Ir  $4f$  peaks of the Pt doped samples have asymmetric line shape due to the increase of conduction electron by the Pt doping. Interestingly, the Ir  $4f$  binding energy of  $\text{IrTe}_2$  is smaller than that of  $\text{CuIr}_2\text{S}_4$  as shown in Fig. 2(a), suggesting that the actual number of Ir  $5d$  electrons of  $\text{IrTe}_2$  (formally  $\text{Ir}^{4+}$ ) is larger than that of  $\text{CuIr}_2\text{S}_4$  (formally  $\text{Ir}^{3.5+}$ ).

Valence-band photoemission spectra of  $\text{Ir}_{1-x}\text{Pt}_x\text{Te}_2$  ( $x = 0.00, 0.03, \text{ and } 0.04$ ) are displayed in Figs. 3(a)-(c). In  $\text{IrTe}_2$ , across the orbital or bond order temperature at  $\sim 250$  K, the spectral weight around  $-0.1$  eV is suppressed instead of that at the Fermi level [Fig. 3(a)]. The spectral weight suppression seems to rapidly disappear with the Pt doping. In order to clarify spectral weight change, we divided the photoemission spectra of  $\text{Ir}_{1-x}\text{Pt}_x\text{Te}_2$  by the Fermi-Dirac function convoluted with a Gauss function of FWHM of 8 meV as shown in Figs. 3(d)-(f). The spectral weight around  $-0.1$  eV of  $\text{IrTe}_2$  is suppressed in the low temperature phase. On the other hand, the spectral weight at the Fermi level is almost preserved across the structural transition at  $\sim 250$  K, consistent with the good metallic behavior of the orbital or bond order state.<sup>5,6</sup> However, this result apparently contradicts with the dramatic suppression of magnetic susceptibility below  $\sim 250$  K.<sup>5</sup>

The spectral weight suppression around  $-0.1$  eV of  $\text{IrTe}_2$  would be consistent with band narrowing due to a kind of band Jahn-Teller effect caused by the bond compression. Under the bond compression along the  $b$ -axis (namely, the orbital or bond order along the  $b$ -axis), the Ir  $5d$   $yz$  band width along the  $b$ -axis is increased and the Ir  $5d$   $xy$  and  $zx$  band width is decreased [see Fig. 1(c)]. If the narrow Ir  $5d$   $xy$  and  $zx$  bands become fully occu-

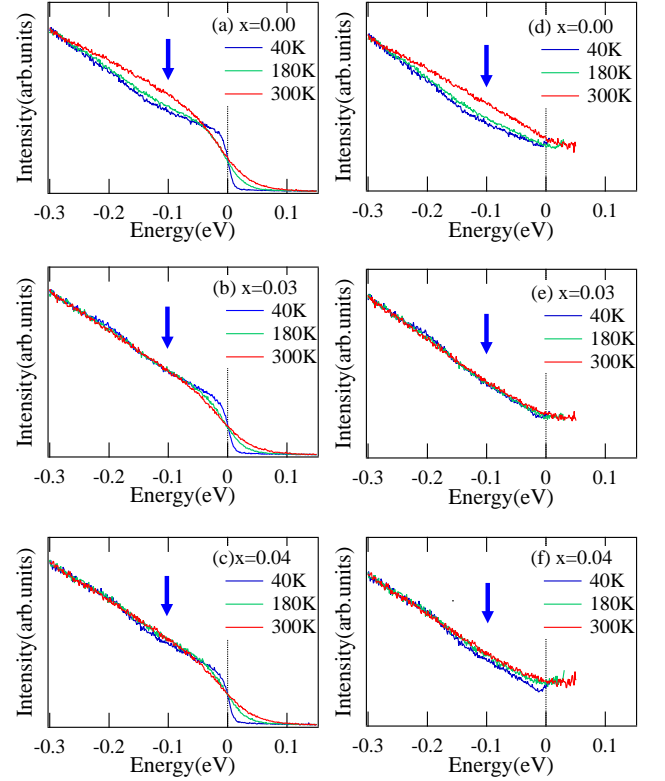


FIG. 3: (color online) Temperature dependent photoemission spectra near the Fermi level of  $\text{Ir}_{1-x}\text{Pt}_x\text{Te}_2$  for (a)  $x = 0.00$ , (b)  $x = 0.03$ , and (c)  $x = 0.04$ . The spectra are taken at photon energy of 10 eV. Temperature dependence of the photoemission spectra divided by the broadened Fermi-Dirac function of  $\text{Ir}_{1-x}\text{Pt}_x\text{Te}_2$  for (d)  $x = 0.00$ , (e)  $x = 0.03$ , and (f)  $x = 0.04$ .

pied and their tops are located below  $\sim -0.1$  eV from the Fermi level, the density of states down to  $\sim -0.1$  eV is expected to be suppressed. This situation can be demonstrated by the tight binding calculation for a multi-band model including the Ir  $5d$  and Te  $5p$  orbitals with realistic transfer integrals and spin-orbit interactions. Using  $\Delta$  of 1.0 eV, the Ir  $5d$  holes are accommodated in the Ir  $5d$   $yz$  orbitals and the density of states from the Fermi level to  $-0.1$  eV is actually suppressed as shown in Fig. 4(a). Figure 4(a) also shows the calculated results without the spin-orbit interaction. Although the effect of the spin-orbit interaction is rather small near the Fermi level (the geometry of the Fermi surface is also the same with and without the spin-orbit interaction), the density of states below  $\sim -0.1$  eV is affected by the spin-orbit interaction. The calculated results for  $\Delta$  of 2.0 eV and  $-2.0$  eV are displayed in Fig. 4(b). The calculated spectral change is too large for  $\Delta$  larger than 2.0 eV, and it is too small for  $\Delta$  smaller than  $-2.0$  eV. The  $\Delta$  value close to 0 eV indicates that the Ir  $5d$ -Te  $5p$  hybridization is substantial although the charge density wave formation of the low temperature phase manifests only in the Ir  $4f$  core level (not in the Te  $3d$  core level). Here, it should be

noted that the orbitally-ordered (or bond-ordered) state is unstable without the lattice distortion in the present model calculation probably because the electron-electron interaction is not included.

With Pt substitution of  $x \geq 0.032$ , the orbital or bond order is suppressed and superconductivity appears.<sup>5</sup> Actually, the spectral weight suppression around -0.1 eV of IrTe<sub>2</sub> almost disappears with the Pt doping. However, the dip structure around -0.1 eV slightly remains in the superconducting sample with  $x = 0.03$  and 0.04 as shown in Figs. 3(b) and (c). Assuming that the dip structure around -0.1 eV is due to the orbital or bond order caused by the band Jahn-Teller effect, the band Jahn-Teller effect weakly affects the density of states of  $x = 0.03$  and 0.04. Even in the superconducting sample with  $x = 0.04$ , the dip structure still remains indicating that Ir<sub>1-x</sub>Pt<sub>x</sub>Te<sub>2</sub> has a kind of phase separation between the superconducting state and the orbital or bond order state.

As indicated by the Ir 4f XPS, the low temperature phase of IrTe<sub>2</sub> is accompanied by weak modulation of Ir 5d  $t_{2g}$  electron density. The charge modulation or charge density wave can be induced by Fermi surface nesting due to the orbital or bond order (namely, due to the band Jahn-Teller effect). This situation is similar to the orbitally-induced Peierls effect proposed for CuIr<sub>2</sub>S<sub>4</sub>.<sup>14</sup> In IrTe<sub>2</sub>, when the orbital (or bond) order is established and the Ir 5d holes are accommodated in the Ir 5d  $yz$  orbitals, the Fermi surface is expected to become more one-dimensional to induce the charge density wave. The effect of orbital (or bond) order on the band dispersion and the Fermi surface geometry is demonstrated in Figs. 4(c), (d) and (e). Without the lattice distortion and the orbital (or bond) order, the Fermi surfaces of the Ir 5d bands are made up from the Ir 5d  $yz$ ,  $zx$ , and  $xy$  orbitals and have the six-fold symmetry as expected from the trigonal structure. Under the compression along the  $b$ -axis and the orbital (or bond) order, the transfer integrals of the  $yz$  orbitals are enhanced and those of  $zx$  and  $xy$  orbitals are reduced. As a result, the Ir 5d band width along the  $k_y$  direction is decreased due to the decrease of  $zx$ - $zx$  and  $xy$ - $xy$  transfer as shown in Fig. 4(c), and the quasi-one-dimensional Fermi surface with  $yz$  character is obtained as shown in Fig. 4(e). Such a quasi-one-dimensional Fermi surface is expected to have instability to charge or spin density wave. In contrast to CuIr<sub>2</sub>S<sub>4</sub><sup>10</sup> and LiRh<sub>2</sub>O<sub>4</sub><sup>15</sup> with full gap opening, the amplitude of the charge density wave is probably not enough to cause band gap opening in the case of IrTe<sub>2</sub>.

#### IV. CONCLUSION

We have studied the electronic structure of a triangular lattice Ir<sub>1-x</sub>Pt<sub>x</sub>Te<sub>2</sub> superconductor. The combination between photoemission spectroscopy and model calculations show that the orbitally-induced Peierls effect on Ir 5d  $t_{2g}$  bands plays important role in the charge and

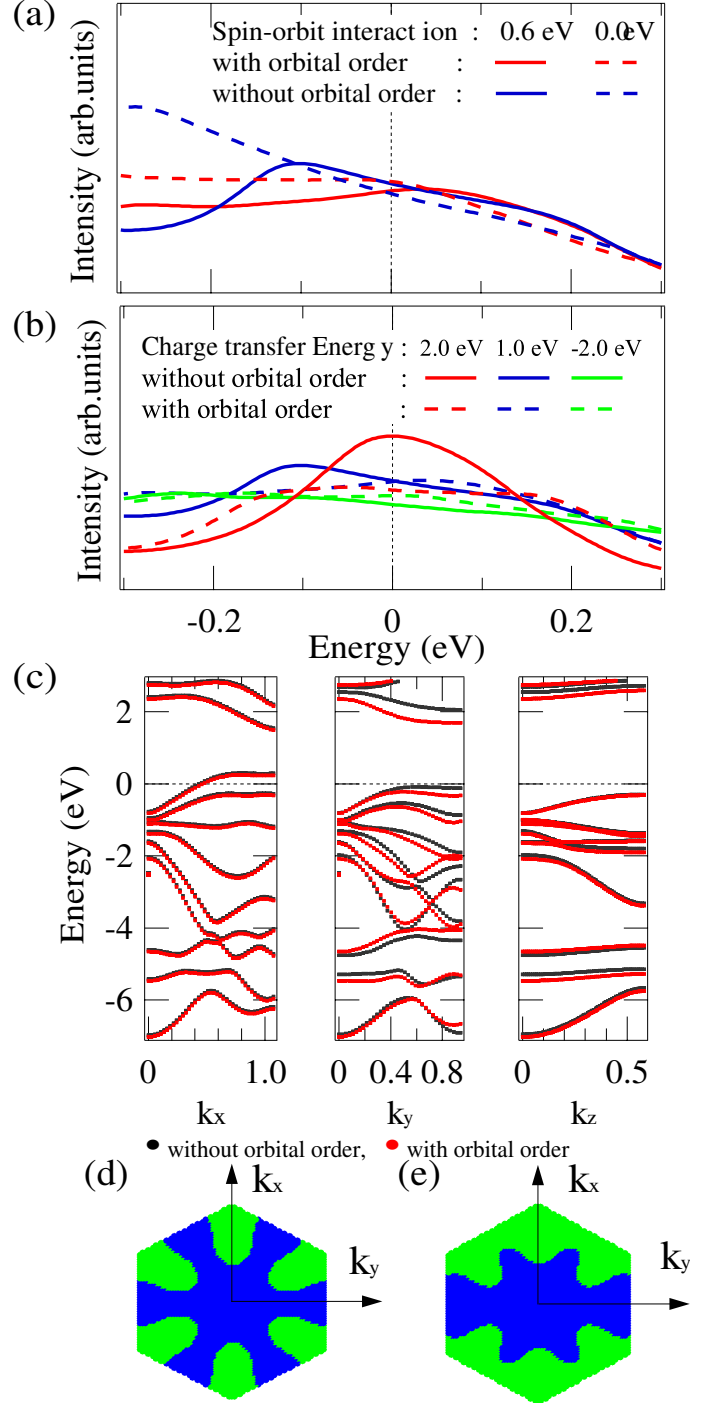


FIG. 4: (color online) (a) The effect of Ir 5d spin-orbit interaction on total density of states near the Fermi level calculated for IrTe<sub>2</sub> with and without orbital (or bond) order.  $\Delta$  is set to 1.0 eV. (b) Total density of states near the Fermi level calculated for IrTe<sub>2</sub> as functions of  $\Delta$  with and without orbital (or bond) order. (c) Band dispersions along the  $k_x$ ,  $k_y$ , and  $k_z$  directions.  $k_x$  and  $k_y$  are parallel to the IrTe<sub>2</sub> plane, and  $k_z$  is perpendicular to it. (d) Fermi surface without orbital (or bond) order. The Fermi surface has the trigonal symmetry due to the orbital degeneracy of Ir 5d  $yz$ ,  $zx$ , and  $xy$  orbitals. The  $k_x$  and  $k_y$  directions are indicated in the figure. (e) Fermi surface with orbital (or bond) order. The Fermi surface becomes quasi-one-dimensional due to a kind of band Jahn-Teller effect to remove the orbital degeneracy of Ir 5d  $yz$ ,  $zx$ , and  $xy$  orbitals. The  $k_x$  and  $k_y$  directions are indicated in the figure.

orbital instability in the IrTe<sub>2</sub>. In the orbitally-induced Peierls mechanism, the Ir 5d t<sub>2g</sub> orbital degeneracy is removed by a kind of band Jahn-Teller effect and the Fermi surface geometry is changed to enhance Fermi surface nesting. The structural change, the resistivity anomaly, and the spectral change across the transition at  $\sim 250$  K in IrTe<sub>2</sub> is well explained by the orbitally-induced Peierls mechanism of the t<sub>2g</sub> electrons on the triangular lattice. However, it is very difficult to explain the drastic suppression of magnetic susceptibility at the transition by the weak charge density wave and the imperfect gap opening. The effect of spin-orbit interaction, which is not included in the simple argument of the orbitally-induced Peierls mechanism, should be included to consider the remaining

mystery. Also the suppression of magnetic susceptibility in IrTe<sub>2</sub> is very similar to that of LiVO<sub>2</sub>, NaTiO<sub>2</sub>,<sup>16</sup> and LiVS<sub>2</sub><sup>17</sup> with 3d electrons which are more localized than the 5d electrons in the Ir compounds. The effect of Mottness should be considered in future theoretical studies.

### Acknowledgement

The authors would like to thank valuable discussions with D. I. Khomskii and H. Takagi. The synchrotron radiation experiment was performed with the approval of HSRC (Proposal No.11-A-7).

- 
- <sup>1</sup> Y. Kamihara, T. Watanabe, M. Hirano, and H. Hosono, *J. Am. Chem. Soc.* **130**, 3296 (2008).
  - <sup>2</sup> H. Takahashi, K. Igawa, K. Arii, Y. Kamihara, M. Hirano, and H. Hosono, *Nature* **453**, 376 (2008).
  - <sup>3</sup> F. C. Hsu, J. Y. Luo, K. W. Yeh, T. K. Chen, T. W. Huang, P. M. Wu, Y. C. Lee, Y. L. Huang, Y. Y. Chu, D. C. Yan, and M. K. Wu, *Proc. Natl. Acad. Sci. U.S.A.* **105**, 14262 (2008).
  - <sup>4</sup> W. Bao, Y. Qiu, Q. Huang, M. A. Green, P. Zajdel, M. R. Fitzsimmons, M. Zhernenkova, S. Chang, M. Fang, B. Qian, E. K. Vehstedt, J. Yang, H. M. Pham, L. Spinu, and Z. Q. Mao, *Phys. Rev. Lett.* **102**, 247001 (2009).
  - <sup>5</sup> S. Pyon, K. Kudo, and M. Nohara, *J. Phys. Soc. Jpn.* **81**, 053701 (2012).
  - <sup>6</sup> N. Matsumoto, K. Taniguchi, R. Endoh, H. Takano, and S. Nagata, *J. Low Temp. Phys.* **117**, 1129 (1999).
  - <sup>7</sup> K. Homma and F. Izumi, *J. Appl. Crystallogr.* **44**, 1272 (2011).
  - <sup>8</sup> C. J. Raub, V. B. Compton, T. H. Geballe, B. T. Matthias, J. P. Maita, and G. W. Hull Jr., *J. Chem. Solids* **26**, 2051 (1965).
  - <sup>9</sup> B. T. Matthias, T. H. Geballe, and V. B. Compton, *Rev. Mod. Phys.* **35**, 1 (1963).
  - <sup>10</sup> S. Nagata, N. Matsumoto, Y. Kato, T. Furubayashi, T. Matsumoto, J. P. Sanchez, and P. Vulliet, *Phys. Rev. B* **58**, 6844 (1998).
  - <sup>11</sup> P. G. Radaelli, Y. Horibe, M. J. Gutmann, H. Ishibashi, C. H. Chen, R. M. Ibberson, Y. Koyama, Y. S. Hor, V. Kirykhin, and S. W. Cheong, *Nature* **416**, 155 (2002).
  - <sup>12</sup> K. Takubo, S. Hirata, J. Y. Son, J. W. Quilty, T. Mizokawa, N. Matsumoto and S. Nagata, *Phys. Rev. Lett.* **95**, 246401 (2005).
  - <sup>13</sup> T. Mizokawa and A. Fujimori, *Phys. Rev. B* **54**, 5368 (1996).
  - <sup>14</sup> D. I. Khomskii and T. Mizokawa, *Phys. Rev. Lett.* **94**, 156402 (2005).
  - <sup>15</sup> Y. Okamoto, S. Niitaka, M. Uchida, T. Waki, M. Takigawa, Y. Nakatsu, A. Sekiyama, S. Suga, R. Arita, and H. Takagi, *Phys. Rev. Lett.* **101**, 086404 (2008).
  - <sup>16</sup> H. F. Pen, J. van den Brink, D. I. Khomskii, and G. A. Sawatzky, *Phys. Rev. Lett.* **78**, 1323 (1997).
  - <sup>17</sup> N. Katayama, M. Uchida, D. Hashizume, S. Niitaka, J. Matsuno, D. Matsumura, Y. Nishihata, J. Mizuki, N. Takeshita, A. Gauzzi, M. Nohara, and H. Takagi, *Phys. Rev. Lett.* **103**, 146405 (2009).